JOURNAL OF GUIDANCE, CONTROL, AND DYNAMICS
Vol. 22, No. 5, September–October 1999

Stability and Control of an Atmospheric Tether with a Lifting Probe

Brian Biswell* and Jordi Puig-Suari†
Arizona State University, Tempe, Arizona, 85287–6106

This paper explores the stability and control of an atmospheric tether system that includes a lifting probe with a moveable attachment point. The dynamics of the system with the tether modeled as a rigid rod are linearized about equilibria for circular equatorial orbits. Examination of the eigenvalues of the linearized system shows that there is always at least one unstable mode that needs to be controlled. A linear control system that uses the attachment point motion and thrust at the orbiter as inputs is shown to be suitable for the conditions considered. The system is also controllable with any single control input.

I. Introduction

In recent years many applications of tethered satellite systems for atmospheric research have been proposed,[1–4] both on the Earth and on other atmosphere-bearing planets in the solar system. Tethers provide many benefits over other means of atmospheric research. For missions around the Earth, they are especially useful at the middle altitudes (about 100–200 km), which are too high for aircraft to reach and too low for sustained study by normal satellites because of drag effects. By tethering a probe to an orbiter that is maintained above the sensible atmosphere, long duration studies of these regions can be made. Tether systems can also be used to obtain atmospheric samples from other planets, to be studied in situ or returned to Earth for further analysis.[3,4]

For a successful atmospheric tether mission a means of controlling the probe altitude should be considered. Proposed control mechanisms have included adjusting the length of the tether[4] and using a hypersonic wave rider.[5,6] The adjustable length mechanism is very slow, generally taking hours to make adjustments, which makes it unsuitable to counter fast perturbations. The wave-rider proposal uses standard aerodynamic control surfaces that add complexity to the probe and have limited control authority.

The authors have previously proposed using a lifting-body probe controlled by means of a moveable attachment point.[7] The probe provides lift that can be used to control the depth of the probe within the atmosphere. In addition, lift on the probe can significantly reduce the length of tether required to penetrate the atmosphere. The moveable attachment point is a simple mechanism, which can be implemented by means of a worm-gear drive or adjustable hawsers as on a kite or parachute.

In Ref. 7 the range of equilibria for various tether lengths and attachment point locations for a Mars sampling mission is explored. In this paper we consider the stability and control of this atmospheric tether system. The results include a controller design for the system using the tether attachment point motion as the sole control input with constant thrust applied at the orbiter.

II. Rigid Nonlinear Model

A typical tether system is composed of an orbiter connected to the atmospheric probe by a long flexible tether. The complete mathematical description of this system is quite lengthy[8] and unsuitable for analytical control system design. For this reason a simplified model is developed that can still provide an understanding of the fundamental behavior of the system. This simple model is based upon the full three-dimensional flexible-elastic model described in Ref. 9, but with many simplifications (see Fig. 1).

First, the motion of the system is restricted to the orbital plane. The orbit is assumed to be equatorial, which removes any atmospheric disturbances that would create out-of-plane motion. Previous results[9] clearly show that these disturbances are small even for nonequatorial orbits, and so can be reasonably ignored.

The orbiter is modeled as a particle for computation of gravity effects, although drag forces are neglected. The gravitational force on the orbiter is

$$F_G = -\mu m/R^2 \tag{1}$$

where μ is the gravitational parameter of the planet and m and R are the mass and orbital radius of the orbiter, respectively. Any thrust required by the tether system (to counter drag effects, for example) is applied at the orbiter. We assume that both the magnitude and direction of the thrust vector can be modulated.

Next, the tether is modeled as a single rigid element. This approximation is valid for a variety of atmospheric tether systems.[1–4] Elasticity, modeled by a spring at the end of the rod, decreases the stability of the tether system.[5] However, the inclusion of a lifting body at the probe can counter this effect,[9] and so, here, the spring has been omitted from the model to reduce complexity.

The calculation of the drag forces acting on the tether requires special consideration. The density of the atmosphere varies along the entire length of the tether. In addition, each point on the tether has a different velocity with respect to the atmosphere. No analytical solution is known for the exact expression of the drag integrals, and so the approximation developed by Biswell et al.[9] is used. This model assumes that the wind direction is constant along the entire length of the tether and that the drag force acts normal to the tether everywhere. The resulting approximate expression for the tether drag is

$$\boldsymbol{F}_{\mathrm{Dt}} = -\tfrac{1}{2}C_{\mathrm{Dt}}\rho d(I_0\omega \times \boldsymbol{B}_1 + I_1\omega \times \boldsymbol{B}_2)(\boldsymbol{v} \times \hat{\boldsymbol{b}}_1) \tag{2}$$

where C_D is the drag coefficient of the tether, ρ is the atmospheric density at the orbiter, d is the diameter of the tether, ω is the rotation rate of the tether with respect to the atmosphere, $\boldsymbol{B}_1$ is the position vector of the tether attachment point of the probe, $\boldsymbol{B}_2$ is the vector from the probe attachment point to the orbiter attachment point, $\boldsymbol{v}$ is the velocity of the center of mass of the tether with respect to the atmosphere, $\hat{\boldsymbol{b}}_1$ is the unit vector aligned along the tether pointing at the orbiter, and

$$I_n = \int_0^{l_t} \xi^n e^{-\xi\cos(\theta_t)/H}\, d\xi \tag{3}$$

where l_t is the length of the tether, θ_t is the angle between the tether and the local vertical, and H is the exponential scale height of the

Received 15 September 1997; revision received 2 December 1998; accepted for publication 11 February 1999.

*Ph.D. Candidate, Department of Mechanical and Aerospace Engineering; currently Member of the Technical Staff, 805/M4, P.O. Box 11337, Raytheon Missile Systems Company, Tucson, AZ 85734-1337; blbiswell@west.raytheon.com. Member AIAA.

†Assistant Professor, Department of Mechanical and Aerospace Engineering; currently Associate Professor, Aeronautical Engineering Department, California Polytechnic State University, San Luis Obispo, CA 93407; jpuigsua@calpoly.edu. Member AIAA.

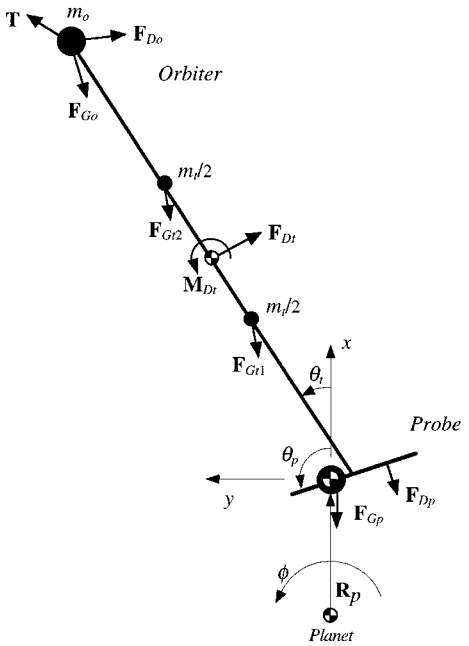

Fig. 1 Simplified tether model.

atmosphere. By integrating along the length of the tether, the aerodynamic moment around the center of the tether is given by

$$M_{\mathrm{Dt}} = -\tfrac{1}{2}C_D\rho d[(I_1 - x_c I_0)(\hat{\boldsymbol{b}}_1 \times (\omega \times \boldsymbol{B}_1)) + (I_2 - x_c I_1)(\hat{\boldsymbol{b}}_1 \times (\omega \times \boldsymbol{B}_2))] \tag{4}$$

where x_c is the distance between the center of mass of the tether to the center of mass of the complete system.

Similarly, the gravity force and moment produced by the inverse-square gravitation law need to be integrated along the entire tether length. However, the analytical expressions for these forces contain singularities that may be solved, but at the expense of increased computation time. Therefore, the mass of the tether is split into two equal point masses, which are located away from the center so as to duplicate the moment of inertia of the rigid rod. This allows the forces and moments to be approximated to within 1%. The resulting gravity force is computed by summing the contribution from each of the two mass elements using Eq. (1).

Finally, the probe (Fig. 2) is modeled as a rigid body composed of a sphere plus a flat plate in order to approximate a general lifting body. The plate has infinitesimal thickness that produces induced drag but no form drag. The sphere is therefore included to model form drag. For the spherical component of the probe, the drag force is given by

$$\boldsymbol{F}_{\mathrm{Ds}} = -\tfrac{1}{2}\rho C_D S|\boldsymbol{v}|\boldsymbol{v} \tag{5}$$

where S is the cross-sectional area of the probe. For the plate, knowledge of the orientation with respect to the local vertical-local horizontal (LVLH) coordinate system is required. Defining the unit vector normal to the plate as $\hat{\boldsymbol{n}}$, the drag on the plate is

$$\boldsymbol{F}_{\mathrm{Dp}} = -2\rho S(\boldsymbol{v}\cdot\hat{\boldsymbol{n}})|\boldsymbol{v}\cdot\hat{\boldsymbol{n}}|\hat{\boldsymbol{n}} \tag{6}$$

Note that the effective drag coefficient of 4 results from the assumption that the plate interacts with the air with full Newtonian reflection.[9]

The attachment point of the tether is assumed to lie on the line between the c.m. of the probe (coincident with the center of the sphere) and the c.p. of the plate. The attitude of the probe is determined by the ratio of the aerodynamic and tension moments about the c.m. This ratio can be described using the nondimensional parameter λ, which is defined by

$$\lambda = \boldsymbol{r}_p/\boldsymbol{r}_{\mathrm{cp}} \tag{7}$$

where $\boldsymbol{r}_p$ is the distance from the c.m. to the tether attachment point (a.p.) and $\boldsymbol{r}_{\mathrm{cp}}$ is the distance from the c.m. to the c.p. (see Fig. 2).

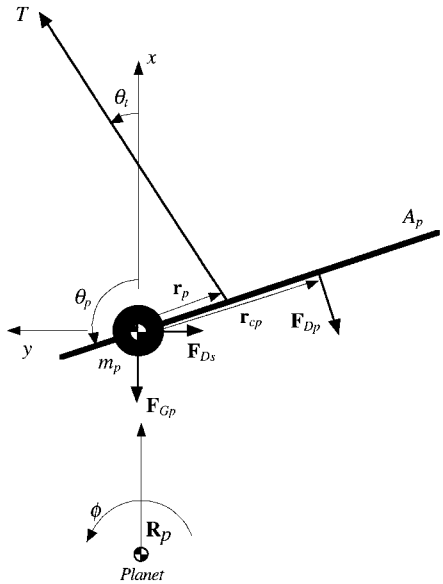

Fig. 2 Probe detail.

This parameter is zero if the a.p. is at the c.m., positive if the a.p. lies between the c.m. and the c.p., and negative if the a.p. is in front of the c.m. When λ is positive, the angle of attack of the probe is negative, and the probe generates negative lift, pulling the system deeper into the atmosphere. Conversely, when λ is negative, the probe generates positive lift and pulls the system out of the atmosphere. In this model, when λ is zero, the induced lift from the probe goes to zero.

The equations of motion for the system are derived by writing Newton's equations for the tether (including the orbiter) and the probe. These equations are

$$m_t\frac{\mathrm{d}^2\boldsymbol{R}_t}{\mathrm{d}t^2} = \boldsymbol{F}_{\mathrm{Go}} + \boldsymbol{F}_{\mathrm{Gt}} + \boldsymbol{F}_{\mathrm{Dt}} - \boldsymbol{T} \tag{8}$$

$$m_p\frac{\mathrm{d}^2\boldsymbol{R}_p}{\mathrm{d}t^2} = \boldsymbol{F}_{\mathrm{Gp}} + \boldsymbol{F}_{\mathrm{Ds}} + \boldsymbol{F}_{\mathrm{Dp}} + \boldsymbol{T} \tag{9}$$

$$I_t\ddot{\theta}_t = M_t + \boldsymbol{r}_o \times \boldsymbol{F}_{\mathrm{Go}} - \boldsymbol{r}_p \times \boldsymbol{T} \tag{10}$$

$$I_p\ddot{\theta}_p = \boldsymbol{r}_{\mathrm{cp}} \times \boldsymbol{F}_{\mathrm{Dp}} + \boldsymbol{r}_p \times \boldsymbol{T} \tag{11}$$

where I_t and I_p are the moments of inertia for the tether and probe, respectively, $\boldsymbol{r}_o$ is the distance from the c.m. of the tether to the tether attachment point on the probe, and $\boldsymbol{T}$ is the tether tension at the probe, which can be eliminated using Eqs. (8) and (9). Note that because the coordinate system shown in Fig. 1 rotates with the tether, the derivatives of the radii are given by

$$\frac{\mathrm{d}^2\boldsymbol{R}}{\mathrm{d}t^2} = \ddot{\boldsymbol{R}} + \dot{\Omega}\times\boldsymbol{R} + 2\Omega\times\dot{\boldsymbol{R}} + \Omega\times\Omega\times\boldsymbol{R} \tag{12}$$

where $\Omega = [0\ \ 0\ \ \dot{\phi}]^T$ is the rotation rate of the coordinate system.

III. Equilibrium Conditions

Figure 3 shows the range of equilibrium probe altitudes achievable by the Mars tether system described in Tables 1 and 2 (these equilibria are based on the Mars mission proposed by Lorenzini, et al.[3] and are discussed in detail in Ref. 7). Figure 3 shows the equilibria for the system with tether lengths from 180 to 300 km and attachment point locations in the range $-1 \le \lambda \le +1$. The orbiter altitude is 300 km for all cases, and the system is maintained in circular orbit. Figure 3 shows that for very short tether lengths (high probe altitudes) changes in λ have little effect on the altitude of the probe. This result is expected because at high altitude the aerodynamic effects on the probe are negligible. As the length of the tether increases, the probe descends deeper into the atmosphere, and aerodynamic effects become more significant on the behavior of the system.

Table 1 Physical parameters for Mars and its atmosphere

Parameter	Value
Radius, R_{planet}	3398 km
Gravitational parameter, μ	4.28×10^4 km^3/s^2
Rotation rate, Ω_P	7.069×10^{-5} rad/s
Reference density, ρ_0	5.5×10^{-8} kg/m^3
Reference radius, r_{ref}	3507 km
Scale height, H	8 km

Table 2 Nominal system parameters

Parameter	Value
Orbiter	
Mass, m_o	1000 kg
Altitude, R_o	300 km
Tether	
Linear density, η	0.3 kg/km
Length, l_t	180–300 km
Diameter, d	0.5 mm
Drag coefficient, C_{Dt}	2
Probe	
Mass, m_p	500 kg
Plate area, A_p	50 m^2
Plate drag coefficient, C_{Dp}	4
Sphere area, A_s	1 m^2
Sphere drag coefficient, C_{Ds}	1

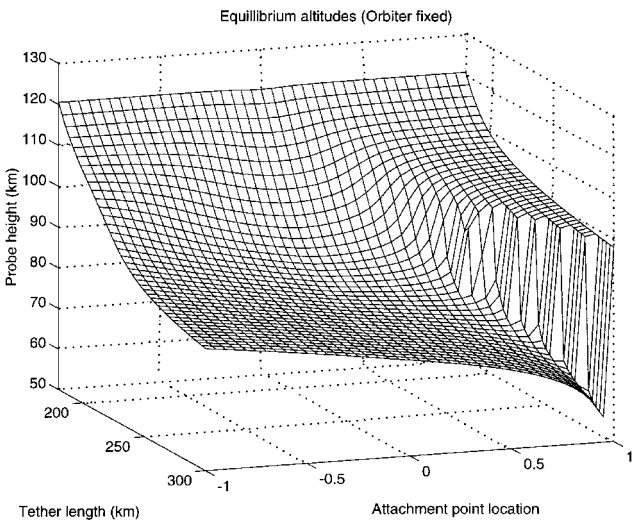

Fig. 3 Equilibrium probe altitudes.

For negative values of λ, the probe generates positive lift, which pulls the probe out of the atmosphere. When $\lambda = 0$, the plate is edge-on to the flow, generating no lift. The equilibrium for this case corresponds to that of the traditional spherical probe model. For small positive values of λ, the plate generates negative lift, thus lowering the probe into the atmosphere. However, as λ approaches $+1$, the probe passes through a transition regime where drag is the dominant force. At this point the attitude of the plate is nearly perpendicular to the flow producing large amounts of drag. This increase in drag generates torques that rapidly pull the probe out of the atmosphere.

IV. Linear Model

The nonlinear model just presented can be analytically linearized using a first-order Taylor expansion about the circular orbit equilibria. In the system there are eight generalized coordinates of interest: the orbital radius of the probe R_p, longitude of the probe ϕ, angles of rotation of the probe and tether θ_p and θ_t, respectively, and their time derivatives $\dot{R}_p$, $\dot{\phi}$, $\dot{\theta}_p$, and $\dot{\theta}_t$. These are the eight states of the linear model. However, the longitude of the probe can be deleted from the system of equations because it does not affect the motion when the system is orbiting a spherical planet. The derivative of the longitude is the orbital angular velocity, which is still required, however. There are three control inputs to the system: the vertical and horizontal components of thrust and the tether attachment point location. Each of these inputs can be modulated about the equilibrium position.

The Taylor expansion was performed symbolically for a general equilibrium condition using Mathematica™. The resulting linear equations were then exported to MATLAB™ where various specific equilibria were evaluated. These equations are very complex, lengthy, and cannot easily provide an analytical control law. Instead, one can perform numerical analysis of specific configurations.

To determine the validity of the linearized model, numerical simulations of the linear and simplified nonlinear models were performed. The simulations for the tether parameters listed in Table 1 with a tether length of 300 km and a fixed attachment point value of $\lambda = 0.5$ are presented here. Figures 4a and 4b compare the results generated by the linear and nonlinear equations of motion for a $+1$-km perturbation of the equilibrium orbital radius. Thrust on the orbiter is fixed at the equilibrium value. Only the probe altitude and angle are shown for compactness. The results show that the two simulations are initially very close, indicating that the linear model is fairly accurate until nonlinear effects become dominant.

In addition, these results clearly show that the system is unstable. The radius is increasing exponentially, with the other states following suit (not shown), until nonlinear effects dominate. This result can be easily predicted because the perturbation places the system at a higher altitude than the equilibrium, where atmospheric density

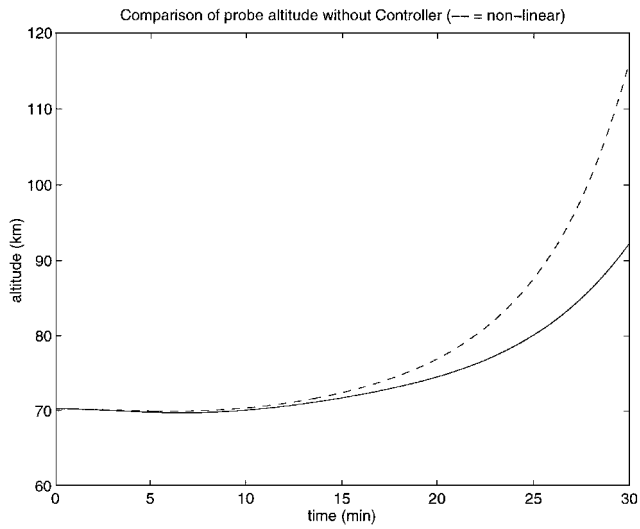

a) Probe altitude

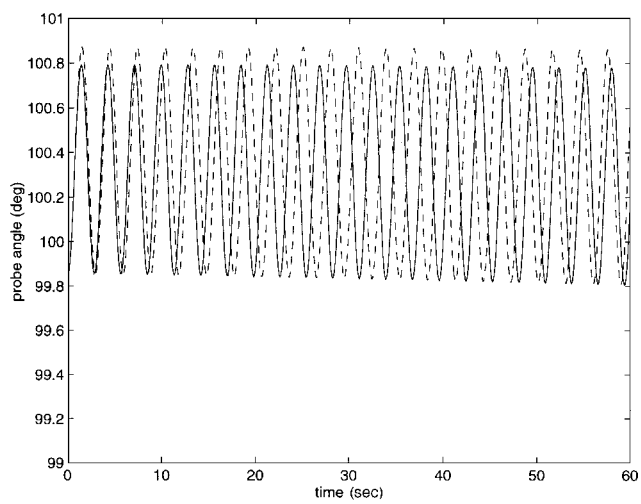

b) Close-up of probe angle

Fig. 4 Comparison of linear and nonlinear system behavior for a 1-km disturbance to the orbital radius.

and drag are lower. Consequently, the thrusters are generating too much thrust, raising the orbit of the system. The opposite effect would occur if a negative radius perturbation had placed the system deeper into the atmosphere.

V. Stability

Given the linear model, the eigenvalues of the system can be used to determine its stability properties. For the configuration simulated in Fig. 4, the seven eigenvalues are

$$6.86 \times 10^{-4} \pm 2.22j$$

$$2.51 \times 10^{-3}$$

$$-1.36 \times 10^{-3} \pm 5.61 \times 10^{-3} j$$

$$-2.50 \times 10^{-4} \pm 1.57 \times 10^{-3} j$$

The first unstable mode is a rapid oscillatory mode associated with the probe attitude (Fig. 4b). The second unstable mode is a purely exponential mode dominated by changes in the altitude of the system (Fig. 4a). The third and fourth modes are stable oscillatory modes. The third mode relates to the coupling between orbital radius and angular velocity whereas the last mode represents the coupling between radius and tether libration. The libration mode has a natural frequency near $\sqrt{3}$ times the orbital rate (9.5×10^{-4} rad/s in this case), a result predicted by linear analysis of the dynamics of rigid bodies in circular orbit.[1] No and Cochran,[6] Keshmiri and Misra,[8] and Onoda and Watanabe[10] all show similar results for tether systems at the Earth, even when the orbiter is much more massive than the probe.

Whereas Fig. 4 shows how one particular equilibrium point behaves, it is instructive to look at the behavior of the whole class of equilibria shown in Fig. 3. By finding the eigenvalues for each of the equilibria, we can generate a root locus plot of all of the system roots vs either tether attachment for a fixed length, or for a range of lengths and a fixed λ. The former is the most instructive and is shown in the following.

We present two cases: a tether length of 300 km, which is indicative of the system behavior at low altitudes, and a length of 210 km, which shows the behavior at higher altitudes. Each of the plots in Figs. 5–9 show the eigenvalues of the system vs values of λ from -1 to $+1$. The roots at $\lambda = -1$ are shown with a X, while those at $\lambda = 0$ are shown with a O. The roots for the λ at which the altitude transition starts are shown with a $+$, and roots for $\lambda = +1$ are shown with a $*$. Because the mode associated with the probe oscillation has a much larger magnitude than the rest of the modes, its roots are shown in a separate plot for clarity.

Figure 5 shows the roots of the plate oscillation mode for the 210-km tether. All of the roots before the transition are lightly damped and oscillatory. After the transition they become purely real. Figure 6 shows a close-up of the oscillating modes of the plate. The plate is stable for $\lambda < 0$. As λ approaches zero, so do the eigenvalues because the plate is coming edge-on into the flow and the aerodynamic lift is going to zero. For positive λ the roots are initially unstable. However, the mode becomes stable again as the transition is approached.

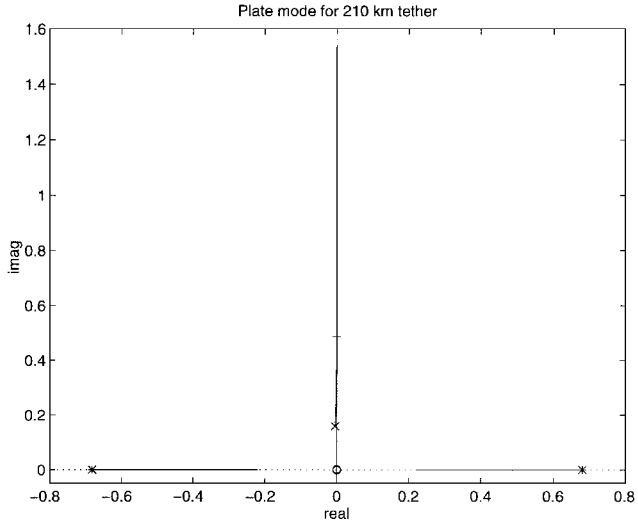

Fig. 5 All roots of the probe oscillation mode for the 210-km tether.

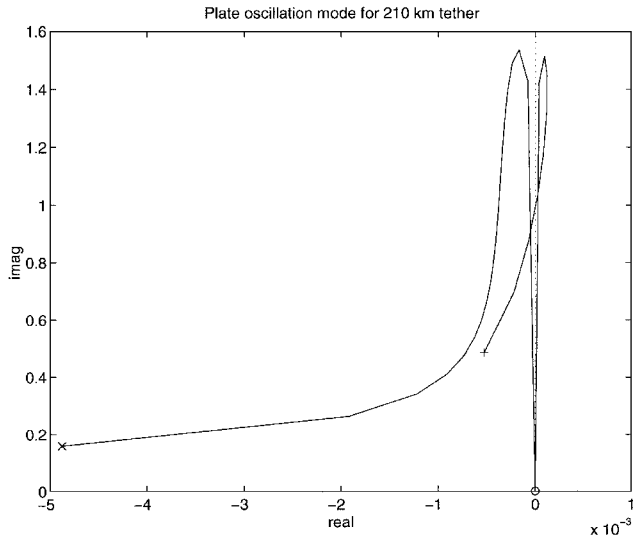

Fig. 6 Roots of the plate mode before transition for 210-km tether.

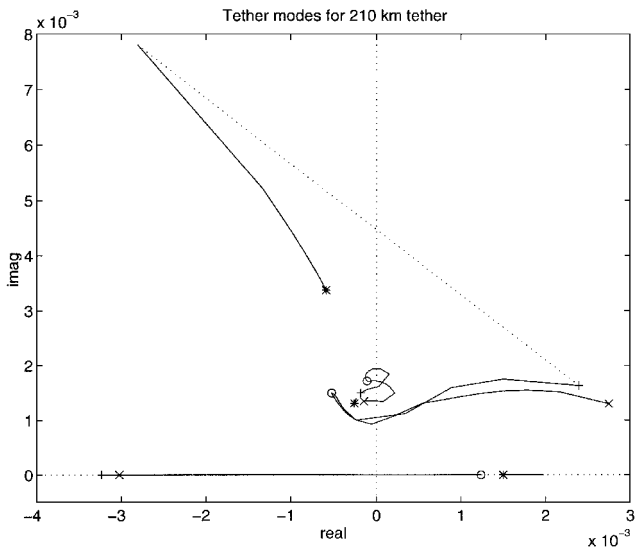

Fig. 7 Roots of the nonplate modes for the 210-km tether.

Figure 7 shows the remaining roots of the 210 km tether. There are two oscillatory modes involving the tether libration and system orbital velocity. The angular velocity mode is the tightly packed set of roots right along the imaginary axis. Both modes move back and forth between stable and unstable regions. After the transition (dotted lines) both modes are stable. The radial mode is purely real, and it too oscillates between stable and unstable. After the transition it remains in the unstable region. For this tether length there is always at least one unstable mode and as many as five for a given λ.

Figure 8 shows the roots of the plate oscillation mode for the 300-km tether. In general, the behavior is similar to that seen in the 210-km tether. Figure 8 shows that the plate motion is stable for all $\lambda < 0$, although extremely lightly damped. As λ approaches $+1$, the roots become unstable. For clarity, the roots after the transition ($\lambda \approx +1$) are not shown on the plot. They are purely real with values of ± 0.34.

Figure 9 shows the remaining roots of the 300-km tether system. The two stable oscillatory modes are the tether libration mode and the orbital velocity coupling mode. These modes have a much higher

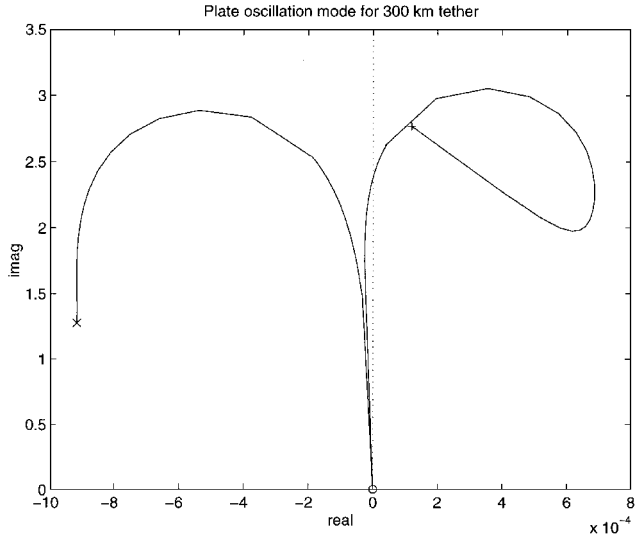

Fig. 8 Roots of the plate oscillation mode for the 300-km tether.

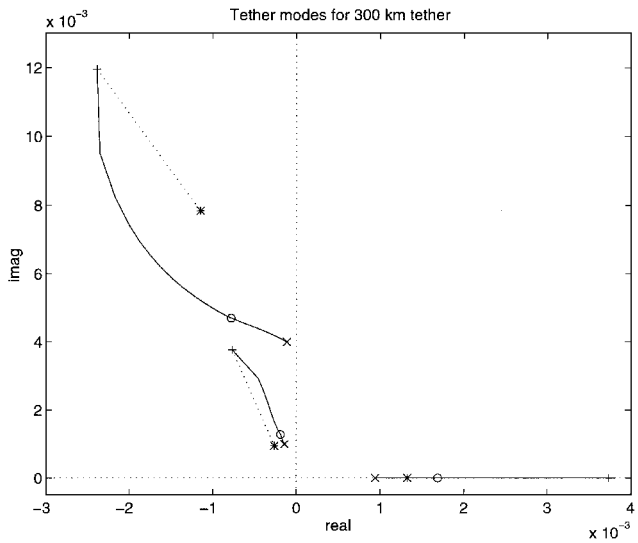

Fig. 9 Roots of the nonplate modes for the 300-km tether.

damping ratio than the plate mode (about 20%). The dashed lines indicate the altitude transition. After the transition these modes have a much lower frequency because of the large change in the system geometry at this point. The positive real root corresponds to the radial mode, which is unstable. An unexpected result is that although the geometric changes to the system are much larger for the 300-km tether the changes in the behavior of the system eigenvalues are more pronounced in the 210-km tether.

These results indicate that there is always at least one unstable mode (and as many as five), and hence some means of control is required. Although we have shown only two tether lengths, they highlight the differences between high-altitude and low-altitude systems.

Overall, the root loci are well behaved over most of the region, with the exception of the altitude transition and the region near $\lambda = 0$. At the transition small perturbations or uncertainties in the system parameters lead to rapidly changing characteristics. On the other hand, near $\lambda = 0$ the control authority of the plate is reduced as lift goes to zero.

VI. Controllability

Controllability of the system is determined by the rank of $\boldsymbol{Q}_c$, the controllability matrix, for the various equilibria. For all of the equilibria shown in Fig. 3, $\boldsymbol{Q}_c$ is full rank, and the system is controllable. The most interesting result, however, is that the system is not just controllable using all three control inputs (vertical and horizontal thrust plus the tether attachment point location), but that it is also completely controllable with any single input, which means that the thrust could be maintained at a constant level and the system controlled purely by adjusting the probe attachment point. This action reduces the complexity of the thruster system on the orbiter and also means that for aerobraking maneuvers,[11] where thrust is not available, the probe can help adjust for variations in the density of the atmosphere. The other possibility is to fix the attachment point and vary the thrust levels on the orbiter. The problems with this approach are two-fold. The thruster would need to be modulated (which is generally not feasible with most thruster systems). It can also lead to a situation where the orbiter must push on the tether to change the probe attitude, which is unrealistic but arises from the rigid tether assumption.

One caveat to the controllability analysis is that these results are valid only in a small region around the equilibrium configuration for the nonlinear model. Within this small region, and for the rigid tether, these results are valid. Outside this region, and for the flexible tether, the nonlinearities quickly build up, rendering the analysis suspect. However, this analysis is still instructive in specifying the general behavior of the tether in circular orbit.

VII. Sample Controller

A. Controller Design

Using the linear model a controller was generated for the tether system already shown. The controller was designed using the linear quadratic regulator (LQR) method with full state feedback. As the system was found to be controllable by any single input, we chose to design the controller using the attachment point motion as the sole input. Note that thrust is still required at the orbiter to keep the system in circular orbit, but is left at the equilibrium values of 212 N and 374 N in the x and y directions, respectively (see Fig. 1). The large thrust levels are required to counter the drag induced by placing the probe at such a low altitude (75 km in this case). However, this is an altitude that could not be reached without using lift from the probe. Also, the thrust requirement can be reduced by maneuvering the probe to higher altitudes (using the moveable attachment point) between sample passes.[12]

For the system used in the simulations (300-km tether with $\lambda = 0.5$ at equilibrium), the states and controls are

$$\boldsymbol{x} = [R_p \quad \theta_t \quad \theta_p \quad \dot{R}_p \quad \dot{\phi} \quad \dot{\theta}_t \quad \dot{\theta}_p]^T, \qquad \boldsymbol{u} = [\lambda] \tag{13}$$

The initial linear equations were poorly scaled and did not provide a suitable solution for the Ricatti equation. Therefore, the equations were normalized to rescale the problem. Lengths were divided by the orbital radius of the probe R_p, velocities by the orbital radius times orbital angular rate $R_p\dot{\phi}$, and angular velocities by the orbital angular rate $\dot{\phi}$. The angles were not rescaled, as they were already of order one.

The normalized equations are

$$\boldsymbol{A} = \begin{bmatrix} 0 & 0 & 0 & 9.5e{-}4 & 0 & 0 & 0 \\ 0 & 0 & 0 & 0 & 0 & 9.5e{-}4 & 0 \\ 0 & 0 & 0 & 0 & 0 & 0 & 9.5e{-}4 \\ -4.7e{-}2 & -1.1e{-}4 & 8.6e{-}4 & 8.3e{-}4 & 2.2e{-}3 & 1.5e{-}5 & -3.5e{-}4 \\ 1.9e{-}2 & 3.8e{-}4 & 1.6e{-}3 & 3.0e{-}4 & -8.0e{-}5 & 2.7e{-}6 & 1.0e{-}10 \\ 3.7e{-}2 & -8.1e{-}3 & -3.2e{-}2 & -4.0e{-}2 & 7.6e{-}4 & 1.1e{-}3 & -2.1e{-}8 \\ 1.5e{+}5 & -5.9e{+}2 & -5.2e{+}3 & -6.2e{+}3 & -5.2e{+}2 & 2.3e{+}2 & -1.2e{-}3 \end{bmatrix} \tag{14}$$

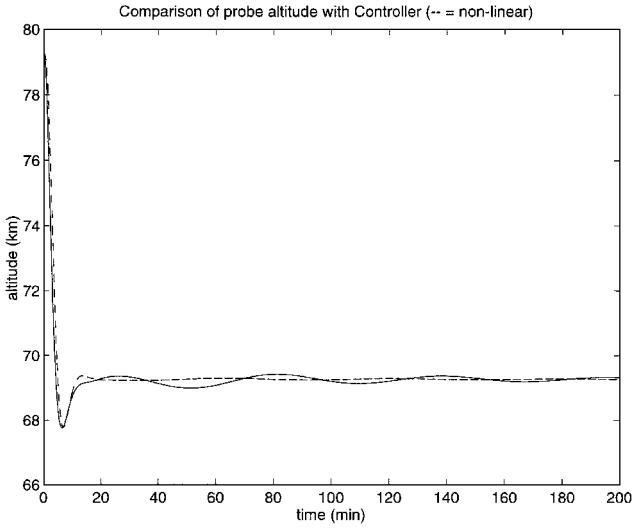

a) Probe altitude

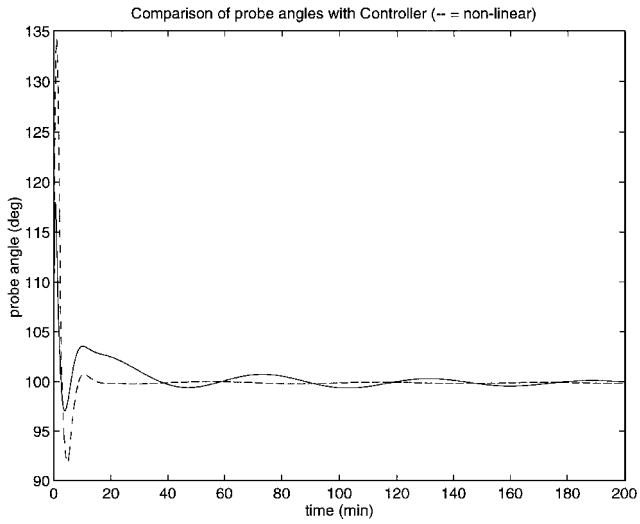

c) Probe angle

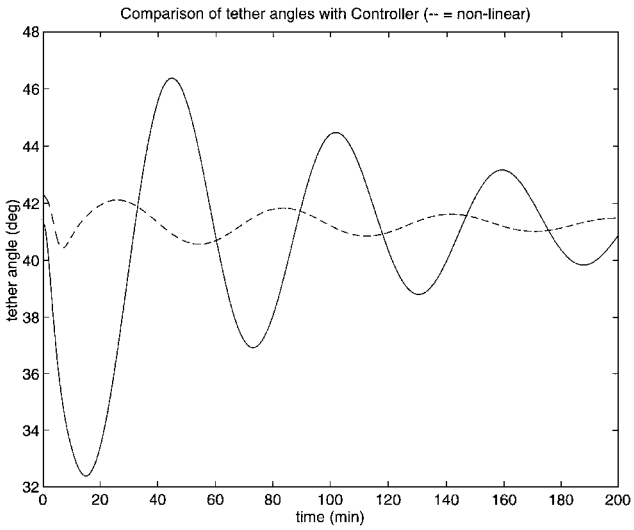

b) Tether libration angle

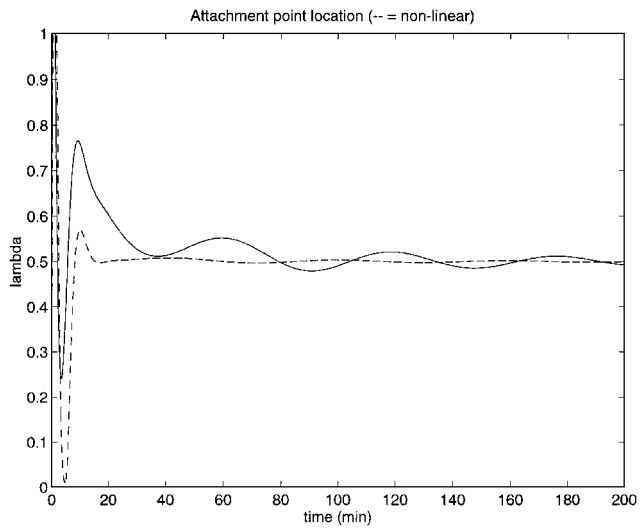

d) Attachment point location

Fig. 10 Controlled tether system response to initial disturbance: ——, linear, and - - - -, nonlinear.

and

$$\boldsymbol{B} = \begin{bmatrix} 0 \\ 0 \\ 0 \\ 7.6e{-}5 \\ 6.5e{-}5 \\ -1.1e{-}3 \\ -2.4e{+}2 \end{bmatrix} \tag{15}$$

We chose the following weight matrices for the normalized system

$$\boldsymbol{Q} = \text{diag}(10^8,\ 10^{-1},\ 10,\ 1,\ 1,\ 1,\ 1), \qquad \boldsymbol{R} = [10] \tag{16}$$

to satisfy the linear quadratic cost function

$$J = \frac{1}{2}\int_0^\infty (\boldsymbol{x}^T\boldsymbol{Q}\boldsymbol{x} + \boldsymbol{u}^T\boldsymbol{R}\boldsymbol{u})\,\mathrm{d}t \tag{17}$$

Note that the weights were chosen to give priority to controlling the altitude of the probe. The resulting controller gains for the original unscaled system are

$$\boldsymbol{K} = [8.4e{-}4\ \ -8.30\ \ -4.36\ \ 0.13\ \ 1.1e{+}5\ \ 2.6e{+}3\ \ -3.3e{+}2]^T \tag{18}$$

B. Simulation Results

Figure 10 shows the results of a simulation of the system using this controller. The initial perturbation was an increase of the probe altitude by 10 km (which represents 1.25 scale heights of the atmosphere). The results from the linear model are shown as a solid line, whereas the same controller applied to the simplified nonlinear two-dimensional model is shown as a dashed line. The attachment point location is saturated at a value of $\lambda = \pm 1$ for the nonlinear simulation to provide a more realistic simulation of the actuator mechanical limits. The controller is able to rapidly bring the probe to the desired altitude and is working to damp out the oscillations of the tether. Note that the oscillations in the nonlinear model are much smaller than in the linear model, probably because of additional damping provided by nonlinear effects in the drag terms. Although there are significant residual oscillations in the tether angle, these are being damped out and represent oscillations in the orbiter altitude. Overall, the simulations show that the controller performs quite well.

C. Atmospheric Disturbances

To study robustness, the controller is applied to the nonlinear system with atmospheric disturbances. The atmosphere is modeled with the same exponential function, but with an exceptionally large 25% diurnal bulge effect. Figure 11 shows the results of this simulation. As can be seen, the probe is still brought rapidly to the desired altitude, with some residual oscillations caused by the atmospheric variations throughout the orbit. The oscillations are less than ± 1 km. Clearly, the controller is able to adequately control the system as desired.

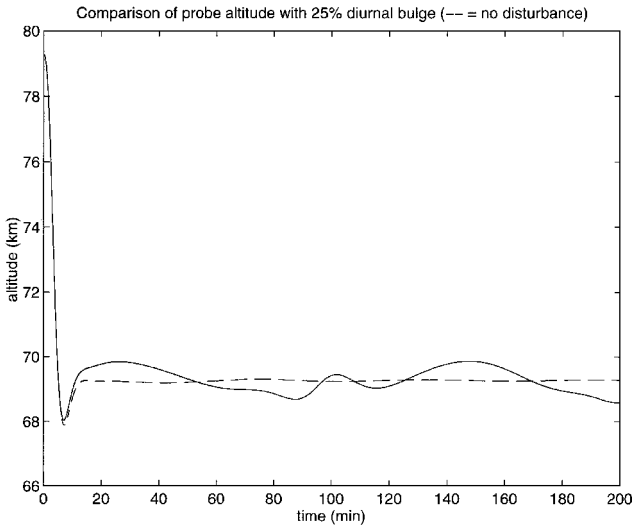

Fig. 11 Effects of controller with 25% diurnal bulge disturbance.

VIII. Conclusions

The atmospheric tether system always contains at least one unstable mode that must be controlled. The controllability tests show that the system is controllable when using the probe attachment point location and horizontal and vertical thrust at the orbiter. Also, the system is still completely controllable when the attachment point motion is the only control input and the thrust is left at the constant equilibrium value. The linear controller design presented here is able to adequately control the system, even with large disturbances and perturbations in the initial conditions. The mechanism presented here shows great potential for the control of atmospheric tether satellite systems.

References

[1]Cosmo, M. L., and Lorenzini, E. C., (eds.), *Tethers in Space Handbook*, 3rd ed., Office of Space Flight Advanced Programs, NASA, Washington, DC, 1997, pp. 37–54.

[2]Bergamaschi, S., and Bonon, F., "Equilibrium Configurations in a Tethered Atmospheric Mission," *Proceedings of the American Astronautical Society/AIAA Astrodynamics Conference*, American Astronautical Society, Paper 91-543, Aug. 1991.

[3]Lorenzini, E., Grossi, M. D., and Cosmo, M., "Low Altitude Tethered Mars Probe," *Acta Astronautica*, Vol. 21, No. 1, 1990, pp. 1–12.

[4]Pasca, M., and Lorenzini, E. C., "Optimization of a Low Altitude Tethered Probe for Martian Atmosphere Dust Collection," *Proceedings of the Fourth International Conference on Tethers in Space*, ThFARp-4, Science and Technology Corp., Hampton, VA, 1995.

[5]Bae, G., Sim, E., and Barlow, J. B., "The Atmospheric Flight Equations of a Tethered Hypersonic Waverider," *Proceedings of the American Astronautical Society/AIAA Spaceflight Mechanics Meeting*, American Astronautical Society, Paper 93-185, Feb. 1993.

[6]No, T. S., and Cochran, J. E., Jr., "Dynamics and Control of a Tethered Flight Vehicle," *Journal of Guidance, Control, and Dynamics*, Vol. 18, No. 1, 1995, pp. 66–72.

[7]Biswell, B., and Puig-Suari, J., "Lifting Body Effects on the Equilibrium Orientation of Tethers in the Atmosphere," AIAA Paper 96-3598, Aug. 1996.

[8]Keshmiri, M., and Misra, A. K., "Effects of Aerodynamic Lift on the Stability of Tethered Subsatellite Systems," *Journal of the Astronautical Sciences*, Vol. 42, No. 3, 1994, pp. 301–318.

[9]Biswell, B., Puig-Suari, J., Longuski, J. M., and Tragesser, S., "A Three Dimensional Hinged-Rod Model for Flexible-Elastic Aerobraking Tethers," *Journal of Guidance, Control, and Dynamics*, Vol. 21, No. 2, 1998, pp. 286–295.

[10]Onoda, J., and Watanabe, N., "Tethered Subsatellite Swinging from Atmospheric Gradients," *Journal of Guidance, Control, and Dynamics*, Vol. 11, No. 5, 1988, pp. 477–479.

[11]Tragesser, S. G., and Longuski, J. M., "The Effect of Parametric Uncertainties on the Aerobraking Tether," AIAA Paper 96-3597, Aug. 1996.

[12]Biswell, B. L., "Active Control of an Atmospheric Tether Using a Lifting Probe," Ph.D. Dissertation, Dept. of Mechanical and Aerospace Engineering, Arizona State Univ., Tempe, AZ, 1998.